| OF |
AD-
A079813

END
DATE
FILMED

2-80

DDC
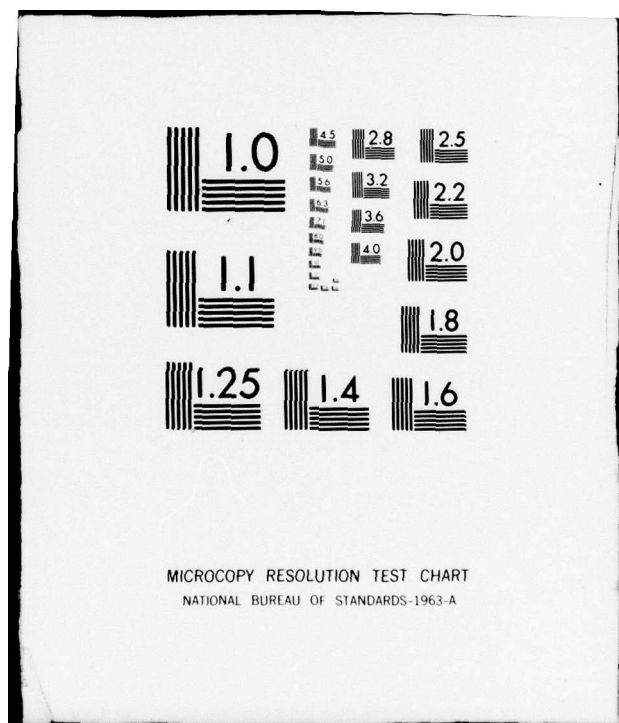
MICROCOPY RESOLUTION TEST CHART
NATIONAL BUREAU OF STANDARDS-1963-A

REPORT DOCUMENTATION PAGE

READ INSTRUCTIONS
BEFORE COMPLETING FORM

1. REPORT NUMBER	2. GOVT ACCESSION NO.	3. RECIPIENT'S CATALOG NUMBER

4. TITLE (and Subtitle)	5. TYPE OF REPORT & PERIOD COVERED
Quantitative Fractography of a Fatigued Ti-28 w/o V Alloy.	Technical Report, 79-1
	6. PERFORMING ORG. REPORT NUMBER

7. AUTHOR(s)	8. CONTRACT OR GRANT NUMBER(s)
Ervin E. Underwood and Saghana B. Chakrabortty	N00014-75-C-0349
031-750

9. PERFORMING ORGANIZATION NAME AND ADDRESS	10. PROGRAM ELEMENT, PROJECT, TASK AREA & WORK UNIT NUMBERS
Fracture and Fatigue Research Laboratory, Georgia Institute of Technology Atlanta, Georgia 30332	27 Nov 79

11. CONTROLLING OFFICE NAME AND ADDRESS	12. REPORT DATE
Metallurgy Program, Material Sciences Div. Office of Naval Research 800 N. Quincy St., Arlington, VA 22217	November 27, 1979
	13. NUMBER OF PAGES
	31

14. MONITORING AGENCY NAME & ADDRESS(if different from Controlling Office)	15. SECURITY CLASS. (of this report)
GIT-TR-79-1	Unclassified
	15a. DECLASSIFICATION/DOWNGRADING SCHEDULE

16. DISTRIBUTION STATEMENT (of this Report)

unlimited

DISTRIBUTION STATEMENT A
Approved for public release
Distribution Unlimited

17. DISTRIBUTION STATEMENT (of the abstract entered in Block 20, if different from Report)

DDC
RECEIVED
JAN 24 1980
A

18. SUPPLEMENTARY NOTES

19. KEY WORDS (Continue on reverse side if necessary and identify by block number)

Quantitative Fractography, Fatigue Crack Growth Mechanisms, Sub-surface cracks, True Facet Area, Fracture Roguhness, Degree of Orientation.

20. ABSTRACT (Continue on reverse side if necessary and identify by block number)

A quantitative fractographic analysis was undertaken to study the micro-structural features important in the understanding of the mechanisms of fatigue crack growth and in the prediction of fatigue crack propagation rates. Special emphasis in this work is placed on the facet characteristics and sub-surface cracking.

The stereological treatment of this problem develops methodologies and relationships based primarily on vertical sections through the fracture surface

DD FORM 1473
1 JAN 73

ADA 079813

DDC FILE COPY

and parallel to the crack propagation direction. The evaluation of fracture profiles (in terms of true length, roughness, and degree of orientation) permits calculation of fracture surface characteristics (such as true surface area, roughness, and type of surface—the latter through an upper-lower bound approach).

True mean facet areas $\bar{A}_t$ are calculated from combined measurements on SEM photographs and vertical sections. The values of $\bar{A}_t$ for the single- and multifacet regions are 22.2 ± 4.9 and 12.7 ± 4.0 n.m^2, respectively, with indicated 95 percent confidence intervals. True mean sub-surface crack lengths $\bar{L}_t$ in the edge section are 0.05 ±0.07/0.05 and 0.16 ± 0.07 mm for the single and multi-facet regions, respectively, while in the center section the corresponding values are 0.13 ± 0.08 and 0.34 ± 0.13 mm. These results reveal that sub-surface cracking under these experimental conditions is a very inhomogeneous process. The types of facets and sub-surface cracks are linked to the local mechanism of fracture, and their characteristics are shown to be consistent with predicted behavior.

QUANTITATIVE FRACTOGRAPHY OF A FATIGUED Ti-28 w/o V ALLOY

by

Ervin E. Underwood[+] and Saghana B. Chakrabortty[++]
Fracture and Fatigue Research Laboratory
Georgia Institute of Technology
Atlanta, Georgia 30332

ABSTRACT

A quantitative fractographic analysis was undertaken to study the microstructural features important in the understanding of the mechanisms of fatigue crack growth and in the prediction of fatigue crack propagation rates. Special emphasis in this work is placed on the facet characteristics and sub-surface cracking.

The stereological treatment of this problem develops methodologies and relationships based primarily on vertical sections through the fracture surface and parallel to the crack propagation direction. The evaluation of fracture profiles (in terms of true length, roughness, and degree of orientation) permits calculation of fracture surface characteristics (such as true surface area, roughness, and type of surface--the latter through an upper-lower bound approach).

True mean facet areas $\bar{A}_t$ are calculated from combined measurements on SEM photographs and vertical sections. The values of $\bar{A}_t$ for the single- and multi-facet regions are 22.2 ± 4.9 and 12.7 ± 4.0 n.m^2, respectively, with indicated 95 percent confidence intervals. True mean sub-surface crack lengths $\bar{L}_t$ in the edge section are $0.05 \pm \begin{smallmatrix} 0.07 \\ 0.05 \end{smallmatrix}$ and 0.16 ± 0.07 mm for the single and multi-facet regions, respectively, while in the center section the corresponding values are 0.13 ± 0.08 and 0.34 ± 0.13 mm. These results reveal that sub-surface cracking

---

[+]Professor of Metallurgy
[++]Senior Research Scientist

80 1 24 026

under these experimental conditions is a very inhomogeneous process. The types
of facets and sub-surface cracks are linked to the local mechanism of fracture,
and their characteristics are shown to be consistent with predicted behavior.

KEY WORDS

Quantitative Fractography, Fatigue Crack Growth Mechanisms, Sub-surface Cracks,
True Facet Area, Fracture Roughness, Degree of Orientation.

INTRODUCTION

Despite the considerable interest expressed over the years in the prediction of fatigue crack growth rates (FCGR), only a few treatments incorporate material constants and no adjustable parameters in their equations.[1,2] In the latest model, Chakrabortty[1] proposes that the cyclic plastic strain at the tip of a propagating fatigue crack, at a given stress intensity range ΔK, depends on the cyclic flow stress and microstructure. Stronger material with a larger effective deformation barrier spacing, λ, has a lower crack tip cyclic plastic strain. The crack growth rate depends on the ability of the material to withstand this plastic strain. In this way, the Chakrabortty equation relates FCGR to a microstructural spacing parameter, the cyclic flow stress, and the cyclic ductility of a material.

In later work, Chakrabortty and Starke[3] demonstrate the accuracy of the Chakrabortty equation. Also, they find that for metastable β Ti-V alloys the fracture features and possibly the cracking mechanisms change as ΔK is varied (see Figure 1). Consequently, they propose mechanisms for each of the three crack growth modes identified in Figure 1. In order to confirm these predictions, additional information is sought in this investigation about the specific microstructure and fracture features that are involved.

According to Figure 1, three regions are observed on the fracture surface. They are identified as multi-facet, single-facet and noncrystallographic in origin. It is postulated[3] that multi-facet crack growth occurs by a decohesion mechanism, and that many decohesion planes are possible in a given grain. Thus, both small facet surfaces and multiple cracking paths become very probable. Single-facet crack growth, on the other hand, is held to occur in conjunction with coarse slip planes; consequently, only one crystallographic facet plane is

favorable in one grain, and the mean facet area approaches the mean cross-sectional area of the grains.

The microstructural and fractographic characteristics of the above two regions should be established quantitatively if at all possible. This paper describes the fractographic study undertaken to establish techniques, develop quantitative relationships, and interpret the data in terms of the crack growth mechanisms.

STEREOLOGICAL ANALYSIS

Quantitative Fractography

A truly quantitative treatment of fracture surfaces would permit one to measure true fracture surface areas, area fractions, sizes and spacings, as well as roughness and orientation characteristics. Central to this undertaking is the ability to determine the true fracture surface area. Methods exist whereby this can be done; but, if possible, we would like to avoid indirect or destructive experimental procedures that are prohibitively laborious or time-consuming. Unfortunately, the standard equations of stereology[4] are not directly applicable in this case because here we are dealing with non-planar surfaces.

A practical objective for such a quantitative treatment would be to base as much of the experimental and analytical procedures as possible on the direct SEM photographs of the fracture surface. These procedures would invoke the basic principles of stereology and projected images[5]. However, with the usual fairly-flat fracture surface, the critical requirement of randomness in the orientation of surface elements is not completely satisfied with one angle of viewing. This problem can be solved, of course, by increasing the number of viewing angles. Moreover, general methods have been worked out to deal with "partially-oriented" surfaces,[6] and the typical fracture surface appears to be another case of such classifications.

Background

The types of direct measurements of three-dimensional features that can be made quantitatively from SEM photographs[7,8,9] and stereoscopic viewing are so rudimentary as to be almost useless for complex, jagged, re-entrant surfaces. Other techniques for obtaining quantitative information from fracture surfaces are interferometry[10] and reflectivity[11] measurements, but these too have limitations. For some materials, microtoming is feasible[12,13]. The resulting profiles can be analyzed or reconstructed into three-dimensional models[14] to yield some insight into the characteristics of the fracture surface as well as its projected image.

Other sectioning techniques are being employed with metallic materials. One way is to section and polish a plane immediately below and parallel to the plane of the fracture surface. Observations made on the fracture surface and in the projection plane can then be compared with the bulk properties revealed by the metallographic section[15,16,17]. This method, of course, is destructive in the sense that the fracture surface is destroyed in order to examine the bulk material underneath.

Sections can also be cut <u>through</u> the fracture surface rather than parallel to it. These may be vertical sections, either parallel or perpendicular to the crack growth direction[18,19], or slanting sections through the fracture surface[20,21,22]. A modification of the latter involves "conical" sectioning, in which a small, selected portion of the fracture surface is surrounded by an etched conical surface extending into the microstructure underneath.[23] This procedure permits the fracture surface to be compared with the microstructure from all directions. However, the region sampled is limited and the etched surfaces are curved, rather than planar.

The fracture profiles obtained by sectioning longitudinally and/or transversely through the fracture surface appear to possess several advantages. First, vertical sections are easily prepared, and measurements on planar sections are straightforward. Moreover, a considerable portion of the fracture surface and underlying alloy is available for statistical sampling and measurements. Most importantly, the linear trace provides an essential quantitative link between accessible two-dimensional measurements and the desired three-dimensional quantities. And finally, with little additional preparation, a direct two-surface visual comparison between fracture profile and fracture surface can be made.

Naturally, there has been considerable activity in the area of quantitative fractography. Recent reviews and publications by Chermant, et al.[24,25,26] and El-Soudani[27-28] have laid much of the groundwork for quantitative treatments. The work of metallurgists, biologists, and instrumentalists have all contributed toward the common goal, even though the original motivations were somewhat different.

Some attempts have been made, especially by Chermant and Coster[24], to systematize the available relationships for quantifying fracture surfaces. This is an extremely difficult task because so many types of relationships are required. For example, to list a few, we need precise relationships that are valid in the fracture surface only, between the fracture surface and projection plane, or between the fracture surface and a parallel plane of polish. If vertical sections are employed, then we need to know the equations relating the fracture surface and its profile and those equations that connect the fracture profile to its projection line. In addition, the basic relationships of projections are required, as well as the appropriate stereological equations for planar sections and projections.

Here we employ the fracture traces obtained from vertical, parallel sections through the fracture surface. Useful relationships and procedures developed specifically for this investigation are described in the appropriate sections below. Primarily, we have tried to account for the lack of complete randomness in the orientation of fracture surface elements in order to assess the true fracture surface area, true facet sizes, and sub-surface crack characteristics.

Vertical Sections

Experimental: A Ti-28 w/o V alloy fatigue specimen was selected for fractographic analysis. Two vertical and parallel longitudinal sections were cut, one near the specimen edge, the other close to the center of the specimen. Figure 2 depicts the positions of the vertical sections and fracture profiles, as well as the locations of the single-facet and multi-facet fracture regions. Typical oblique SEM views are shown of the fracture surface and vertical sections according to location on the fracture surface. Note the large facets in the single-facet regions.

The fracture surface was first electroplated with a layer of copper, then the specimen was mounted and prepared metallographically to show the fracture trace and underlying microstructure near the edge of the specimen. Figure 3 shows examples of the fracture trace from the single- and multi-facet regions. A sequence of photomicrographs were taken along the fracture trace, then assembled into one continuous strip for analysis. The photostrip was marked off into 40 equal lengths, or compartments, for local sampling. This procedure was repeated for a vertical section near the center of the specimen.

Two types of quantities were obtained from each compartment--the true trace length, L_t, and the rose-of-the-number-of-intersections (or simply, the "rose"). The trace lengths were measured in two ways. The first method used a plastic sheet marked with a grid of parallel test lines, giving P_L as a function of

angle within each compartment, at 12 different positions 15° apart. The trace length was then calculated according to[29]

$$L_t = (\pi/2) \; \overline{P_L (\theta)} \; A_T \tag{1}$$

where $\overline{P_L (\theta)}$ is the number of intersections of the trace with the test grid, per unit length of grid, averaged over all 12 angular positions. A_T is an arbitrary test area enclosing the fracture trace within the compartment.

The trace lengths were also measured using the semi-automatic Zeiss MOP-3 operator-interactive image analysis system.[30] Here, the values of L_t are obtained directly and rapidly simply by tracing the fracture profiles with the electronic pencil.

The other experimental quantity obtained from the fracture trace within each compartment is the rose, with angular measurements made as indicated above. Here, however, we need the average values obtained at each angle, over the appropriate number of compartments. The results are plotted as solid lines in Figure 4, in four categories according to whether the data originate within the single- or multi-facet regions or along the edge or center trace. We will return to Figure 4 later.

Calculations: The primary quantity calculated from the above measurements of L_t is the ratio L_t/L', called the lineal roughness parameter R_L by Gurland.[18] $(L_t)_i$ is the true length of the fracture trace in compartment $\underline{i}$, while L' is the projected width (equivalent here to the width of the compartment measured along the mean crack propagation direction (CPD)). Thus, the "rougher" the fracture trace, the larger the value of R_L.

The results of these measurements are presented in Figure 5 for the edge and center sections as well as the single- and multi-facet regions. The average values of R_L for the two traces are 1.06 in the single-facet regions and

1.15 in the multi-facet regions, which amount to about an 8 percent difference. It is noteworthy that the averages of R_L agree as closely as they do ($\pm$ 0.001) between edge and center traces, because manual methods were employed for the edge trace measurements, and the semi-automatic MOP-3 used for the center trace. Based just on these trace length measurements, it would seem that edge effects are absent; at least, for this alloy, fatigued under these conditions, and for this type of specimen geometry. However, as we shall see, other parameters indicate real differences between other trace attributes from section to section and from region to region. In any event, R_L is a valuable parameter in its own right, and plays an important role in calculations of fracture surface areas and facet areas.

The second major quantity calculated from the fracture profile is the rose for the edge and center traces, within the single- and multi-facet regions. The experimental curves (solid lines) are given in Figure 4 along with the results of a least-squares analysis (dashed lines) based on the theoretically-exact equation[6]

$$P_L(\theta)_i = a + b \sin\theta_i \qquad (2)$$

This expression applies to a partially-oriented line in a plane and embodies the assumption that the small linear segments comprising the line are either completely random or fully oriented (parallel to the CPD). The constant a represents the radius of the $P_L(\theta)$ circle centered at the origin (which describes the completely random linear segments), while the b $\sin\theta_i$ term gives two $P_L(\theta)$ circles tangent to the origin (which characterize the fully oriented system of linear segments). The vectorial summation of the circular figures results in the complete roses shown in Figure 4.

Comparisons of the experimental and least-squares roses reveal a slight tendency to peak toward the 90° direction. This probably means that complete orientational randomness is not achieved in the subset of "random" linear segments, but rather in this fairly-flat fracture trace there is an undue proportion of linear segments lying parallel or close to the reference line.

A quantitative index for evaluating the degree of orientation of a line in a plane is Ω_{12}, which is defined by

$$\Omega_{12} = \frac{(P_L)_\perp - (P_L)_\parallel}{(P_L)_\perp + 0.571 (P_L)_\parallel} \; . \tag{3}$$

Here we need only the P_L values perpendicular and parallel to the orientation direction. For a completely oriented line, $\Omega_{12} = 1$, while for a completely random line, $\Omega_{12} = 0$. The intermediate values of Ω_{12} indicate quantitatively the proportion of linear segments oriented parallel to the orientation direction.[6]

The results of the Ω_{12} calculations are reproduced in Table I for both the experimental data and the least squares curves. It is clear that the degree of orientation is higher (by 25-28%) in the single-facet region than the multi-facet region. Moreover, the degree of orientation is generally higher (by 13-17%) in the center trace than in the edge trace. Also noteworthy is the fact that the spread between single-facet and multi-facet data is large along the edge trace, while the comparable data along the center trace show a relatively small spread.

Thus, although the lineal roughness parameter R_L indicates negligible differences in average trace lengths between edge and center traces, the degree of orientation Ω_{12} shows definite differences between these traces. Obviously one parameter is insufficient to completely represent the fracture trace characteristics. In fact, both the rose and the degree of orientation, as well

TABLE 1.

Degree of Orientation Ω_{12} of Fracture Traces in Single-Facet and Multi-Facet Regions of Fatigued Ti-28 w/o V Alloy

	Experimental Data		Least-squares Data	
	Single-Facet	Multi-Facet	Single-Facet	Multi-Facet
Edge Trace	0.676	0.389	0.691	0.470
Center Trace	0.644	0.562	0.754	0.610
Overall Averages (Both Traces)				
	0.660	0.476	0.723	0.540

as R_L, provide the essential information needed for determining the type and extent of fracture surfaces and their areas.

Fracture Surface Area

Ultimately, of course, we would like to relate measurements made on vertical SEM pictures of the fracture surface to true spatial quantities in the fracture surface. As a first step toward this objective, we use vertical longitudinal sections lying parallel to each other and the CPD.

As pointed out above, a complete set of general equations that relate measurements in the projection plane and vertical section to the fracture surface is not yet available. Except in the simplest of cases, exact calculations are not possible, so we have attempted to establish upper and lower bounds that will help to identify the type of fracture surface under scrutiny.

We start the analysis with a definition of fracture surface roughness, S_A, expressed as

$$S_A = S_t/A_T' \tag{4}$$

where S_t is the true fracture surface area (in 3-d space) and A_T' is the projected (test) area (in a 2-d plane) as seen in the SEM picture. Obviously, for a constant projection area there can be a wide range of true fracture surface areas, with $S_t \geq A_T'$. As the true fracture surface area increases (gets "rougher"), the parameter S_A will also increase. Several limiting cases are calculable: for example, $S_A = 2$ for an open surface whose projected area, averaged over all angles, is known. If reentrancies and self-overlap occur, the more general concept, the mean total projection, may be required.

We look next for a direct relationship between the fracture surface area and the trace length in a vertical section through the fracture surface. For our model, we take a test cube of volume $V_T(=L_T^3)$ enclosing a portion of the fracture surface whose projected area A_T' $(= L_T^2)$ is related to the test volume

through $V_T = A'_T L_T$. The trace length in one side of the cube, L_A, is equal to L_t/L_T^2.

Accordingly, we can write

$$\frac{S_t}{A'_T} = \frac{(S_V)_{fracture}}{(A_V)_{projected}} = \frac{(4/\pi)(L_A)_{trace}}{A'_T/V_T} = \frac{4}{\pi}\frac{L_t/L_T^2}{1/L_T} = \frac{4}{\pi}\frac{L_t}{L_T} , \tag{5}$$

where $S_V = (4/\pi)L_A$ is one of the basic equations of stereology, and whose validity for any type of surface depends only on adequate sampling and measurements. Since L_T in this case is also equal to L', the edge length of the projected area, we have

$$S_A = \frac{4}{\pi}\frac{L_t}{L'} = \frac{4}{\pi} R_L \tag{6}$$

where R_L is the lineal roughness parameter defined above. Also, the true surface may be obtained from

$$S_t = \frac{4}{\pi} R_L A'_T \tag{7}$$

where A'_T is the arbitrary projection area with dimensions consistent with our choice of L'.

In order to insure adequate randomness in the sampling of the trace, intersection counts of $P_L(\theta)$ were obtained as described above at 12 angular positions, then averaged for each compartment. Moreover, to provide some three-dimensional coverage, the results for S_A from the two vertical sections were also averaged. The values obtained in this way for the single-facet and multi-facet regions are: $(S_A)_{SF} = 1.32$ and $(S_A)_{MF} = 1.45$. Future experiments are planned that will include additional sections at other angles and in other directions in order to improve randomness in the spatial sampling. By proper utilization of any symmetry elements, however, the number of sections required can be held to a minimum.

The results reported above in Table I demonstrate conclusively that there
is a significant degree of preferred orientation in this fracture surface.
Accordingly, we can utilize the procedures worked out for "systems of partially-
oriented surfaces" as described in the literature[6]. These classifications
include partially-oriented systems of surfaces with linear or planar orientations,
which may apply to our fracture surface.

One method for determining whether the fracture surface belongs to any
particular category of surfaces is to use upper and lower bounds, based on
assumed types of surfaces. This was done here, with the results shown in
Figure 6. Four types of surfaces are evaluated: Minimum, Random, Planar, and
Linear. The pertinent equations for these four cases are as follows:

Case I. Minimum Surface Area. These are ruled surfaces, perpendicular
to the vertical trace, which can have any degree of complexity.

$$(S_V)_{\perp} = L_A = (\pi/2) \ \overline{P_L(\Theta)} \tag{8}$$

where $(S_V)_{\perp}$ refers to fracture surfaces perpendicular to the vertical sec-
tioning plane, L_A is the trace length per unit area in the vertical section,
and $\overline{P_L(\Theta)}$ is the number of intersections of the trace with the grid, per unit grid
length, averaged over angular positions of the test grid. Note that we do not
refer here to the case of a perfectly flat surface.

Case II. Random Fracture Surface. Here we hypothesize a surface with
elements oriented randomly in all directions.

$$S_V = \frac{4}{\pi} L_A = 2 \ \overline{P_L(\Theta)} \tag{9}$$

which applies to any type of surface, as well as a completely-random one, so
long as sampling is sufficient.

Case III. Partially-oriented Surface with Planar Orientation. The surface elements here are relatively flat and equiaxed, and lie mostly parallel to the mean fracture plane.

$$(S_V)_{pl} = (P_L)_\perp + (P_L)_{\parallel} \qquad (10)$$

where the subscripts $\perp$ and $\parallel$ refer to directions taken with respect to the CPD in the vertical section.

Case IV. Partially-oriented Surface with Linear Orientation. These surface elements are not equiaxed, but show some degree of elongation in the CPD.

$$(S_V)_{lin} = \frac{\pi}{2}(P_L)_\perp + 0.429(P_L)_{\parallel} \qquad (11)$$

where $\perp$ and $\parallel$ refer to directions as described above.

The results obtained for these four classes, based on the experimental data, are given in Figure 6 in terms of S_A. The width of each band is determined by the edge- and center-trace values.

The calculations for the first two cases are straightforward and based on well-known equations of stereology. Cases III and IV apply to partially-oriented surfaces with assumed planar and linear orientation. The latter two categories include some fraction of randomly-oriented surface elements, determined experimentally by $(P_L)_\perp$ and $(P_L)_{\parallel}$ from the rose plots.

Our "best" values of S_A, 1.32 for the single-facet and 1.45 for the multi-facet regions, are well within the upper and lower bounds established by the Linear and Minimum bands, respectively. Moreover, these "best" values also lie close to their Planar bands, and thus it appears reasonable to assume that this particular fracture surface belongs more to the planar category of partially-oriented surfaces than the others.

A slightly different interpretation is possible, however, based on the roses obtained from a least-squares analysis of the experimental rose data. As reference to Figure 4 reveals, the least squares curves (dashed lines) are more regular than the experimentally-determined roses (solid lines). Upper and lower bounds calculated from the least-squares data yield a diagram qualitatively similar to that shown in Figure 6, except that the relative positions of the four bands in the single- and the multi-facet regions have shifted somewhat (in general, downward) with respect to the two "best" values of S_A. The latter now lie immediately <u>above</u> their Random bands on the Linear side. Thus, these results would indicate that the fracture surface is best described as mostly random with some tendencies toward linear characteristics. Linear features are evident in SEM photomicrographs of the single-facet region but not in the multi-facet region. Based on this evidence alone it would be difficult to decide between planar or linear structures. However, the experimental data are probably more indicative of the actual state of affairs, so without a more definitive analysis it appears that the planar orientation is more probable.

Facet Areas

One of the more important microstructural features in this investigation are the facets observed in the fracture surface. Since they can be identified in the SEM photostrip, the mean projected area, $(\overline{A'})_{facets}$, may be determined by

$$(\overline{A'})_{facets} = A'_A / N'_A \tag{12}$$

where $A'_A = P'_P$ and N'_A is the number of facets per unit area in the SEM photographs (the projection plane). A'_A can be obtained either manually, with a square point

count grid marked on a plastic sheet, or with the semi-automatic MOP-3 in case
a size distribution of facet areas is required.

The values of $(\overline{A'})_{facet}$ were obtained manually then corrected to true mean
facet areas by a relationship developed for this case. Basically, we postulate
that the projection ratio S_A for the entire fracture surface should equal the
corresponding projection ratio for a selected feature in the fracture surface
(namely, $(A_A)_{facets}$). Accordingly, we write

$$(S_A)_{fracture} = (A_A)_{facets} \tag{13}$$

where $(A_A)_{facets}$ is defined by

$$(A_A)_{facets} = \overline{A}_{facets}/(\overline{A'})_{facets} \tag{14}$$

which is simply a ratio of true mean facet area to the mean projected area.
From this follows

$$\overline{A}_{facets} = (S_A)_{fracture} (\overline{A'})_{facets} \tag{15}$$

or finally

$$\overline{A}_{facets} = \frac{4}{\pi} R_L (\overline{A'})_{facets} \tag{16}$$

which utilizes Eq. (6).

The true mean facet areas measured at 14 positions along the SEM photo-
strip are plotted in Figure 7 as a bar graph. Average values for the single-
and multi-facet regions are indicated, and reveal that the mean facet size in
the single-facet region is almost twice that in the multi-facet region. The
choice and delineation of facet areas in the SEM photostrip is a highly sub-
jective operation, so better experimental methods must be devised to insure
better reproducibility. It should be noted that some results obtained for
the fracture surface also apply to the facet areas; namely the fracture

surface roughness S_A, the degree of orientation, and the identification with planar orientation.

Sub-Surface Cracks

Because sub-surface cracks were noticeably more prevalent in the multi-facet region (see example in Figure 3), methods were investigated for their quantitative characterization. The crack traces are exposed in the vertical sections much the same as the fracture surface traces, so procedures generated for the fracture surface are equally applicable to crack surfaces. A lineal crack roughness parameter for crack traces, similar to the lineal roughness parameter R_L for fracture surface traces, was deemed useful, as well as the true total crack length and a crack surface roughness parameter similar to S_A for the fracture surface.

Crack lengths were determined in two ways: manually, with a grid of parallel lines on a plastic sheet much as described above for measurements of fracture surface trace lengths, and semi-automatically, simply by tracing the crack profile with the MOP-3 electronic pencil. Results of the calculations are summarized in Table II. Note that $(R_L)_{cracks} \geq 0$ is possible, whereas $(R_L)_{trace} \geq 1$.

Several interesting observations can be made from the data in Table II. The multi-facet region has a mean crack roughness parameter about three times greater than that in the single-facet region. Also, the total crack length in the multi-facet region is 4-5 times greater than in the single-facet region. Comparisons between the two traces show that the mean value of the $(R_L)_{cracks}$ parameter for the center trace is about 2.5 times greater than for the edge trace. Thus, sub-surface cracking appears to be a very inhomogeneous process indeed, and one that is linked to the facet sizes and local mechanisms of fracture. If interest dictates, a more detailed study is possible of crack

TABLE II

Parameters for Sub-surface Cracks in Fatigued Ti-28 w/o V Alloy

	Single-facet Region (3.75mm long)	Multi-facet Region (6.25mm long)
I. Mean Lineal Crack Roughness Parameter, $(R_L)_{cracks}$		
Edge trace:	$0.206 \pm \begin{smallmatrix}0.28\\0.21\end{smallmatrix}$	0.654 ± 0.26
Center trace:	0.526 ± 0.30	1.364 ± 0.50
II. Total Sub-surface Crack Trace Length, $\sum_{i=1}^{40} (L_t)_i$		
Edge trace:	0.773mm	4.085mm
Center trace:	1.973mm	8.528mm
III. Mean Crack Surface Roughness Parameter, $(S_A)_{cracks}$		
Edge trace:	$0.262 \pm \begin{smallmatrix}0.36\\0.26\end{smallmatrix}$	0.833 ± 0.33
Center trace:	0.670 ± 0.38	1.737 ± 0.64

branching, orientation, curvature, etc. This is a major field of analysis in itself and much more can be done in this direction.

The results of the local measurements of $(R_L)_{cracks}$ are presented graphically in Figure 8. Although sub-surface cracks are seen to occur irregularly over much of the specimen, the bulk of the cracking, and the greatest intensity of cracking, occurs in the multi-facet region.

DISCUSSION

To put the preceding fractographic analysis in proper perspective, we restate the essential features of the proposed crack growth mechanism[3].

Multi-faceted growth occurs by a decohesion mechanism in front of the crack tip, and numerous decohesion planes are possible in a given grain. As a result, the fracture surface appears to have small, ill-defined cleavage facets which are somewhat smaller than the grain size. Moreover multiple sub-surface crack branching is prevalent because of the multiplicity of decohesion planes. Even though the growth is crystallographic, no single path is preferred. This type of crack growth occurs along AB in Figure 1.

Faceted crack growth is characterized by large, single facets which usually extend across an entire grain. It is postulated that single facets occur by shear-off along two intersecting coarse slip bands at the crack tip. The degree of slip in each of the intersecting slip systems determine the resultant facet orientation. The most efficient facet plane in any given grain will be almost parallel to the crack growth direction. This single facet plane will be favored in the grain. Also, as a result the facets will have a larger degree of orientation and the mean facet area will be close to the mean grain cross-sectional area. The transition from multi-faceted to faceted growth corresponds to region BC in Figure 1; however, faceting persists up to Point D.

Several distinct microstructural characteristics can be expected as a consequence of the proposed mechanisms. We should find that the multi-facet fracture surface:

1. has a lower degree of orientation,

2. has higher roughness parameters,

3. has greater true fracture surface area,

4. has a smaller mean facet size, and

5. has more sub-surface cracking,

all with respect to the single-facet fracture surface. These expectations have been confirmed quantitatively by the present study.

The parameters obtained in our quantitative fractographic study vary from the center trace to the edge trace. This is to be expected, because we change from a plane strain to plane stress condition as we move toward the edge. Under a pure plane stress condition, fracture normally occurs along shear lips. Therefore, we observe a change in the values of degree of orientation, roughness parameter and sub-surface cracking near the edge of the specimen.

CONCLUSIONS

The experimental procedures utilized in this investigation are quite laborious and not well-suited for routine quantitative evaluation of fracture surfaces. However, it is hoped that experience gained here will shorten the time and labor required in subsequent work without appreciably diminishing the accuracy of the results.

With further developments in the quantitative analysis of fracture surfaces, further advances can be anticipated in the formulation of meaningful, quantitative theories for predicting FCGR. Perhaps the greatest contribution from a truly

quantitative fractography would be to find hidden microstructural effects that would normally be overlooked in a qualitative study.
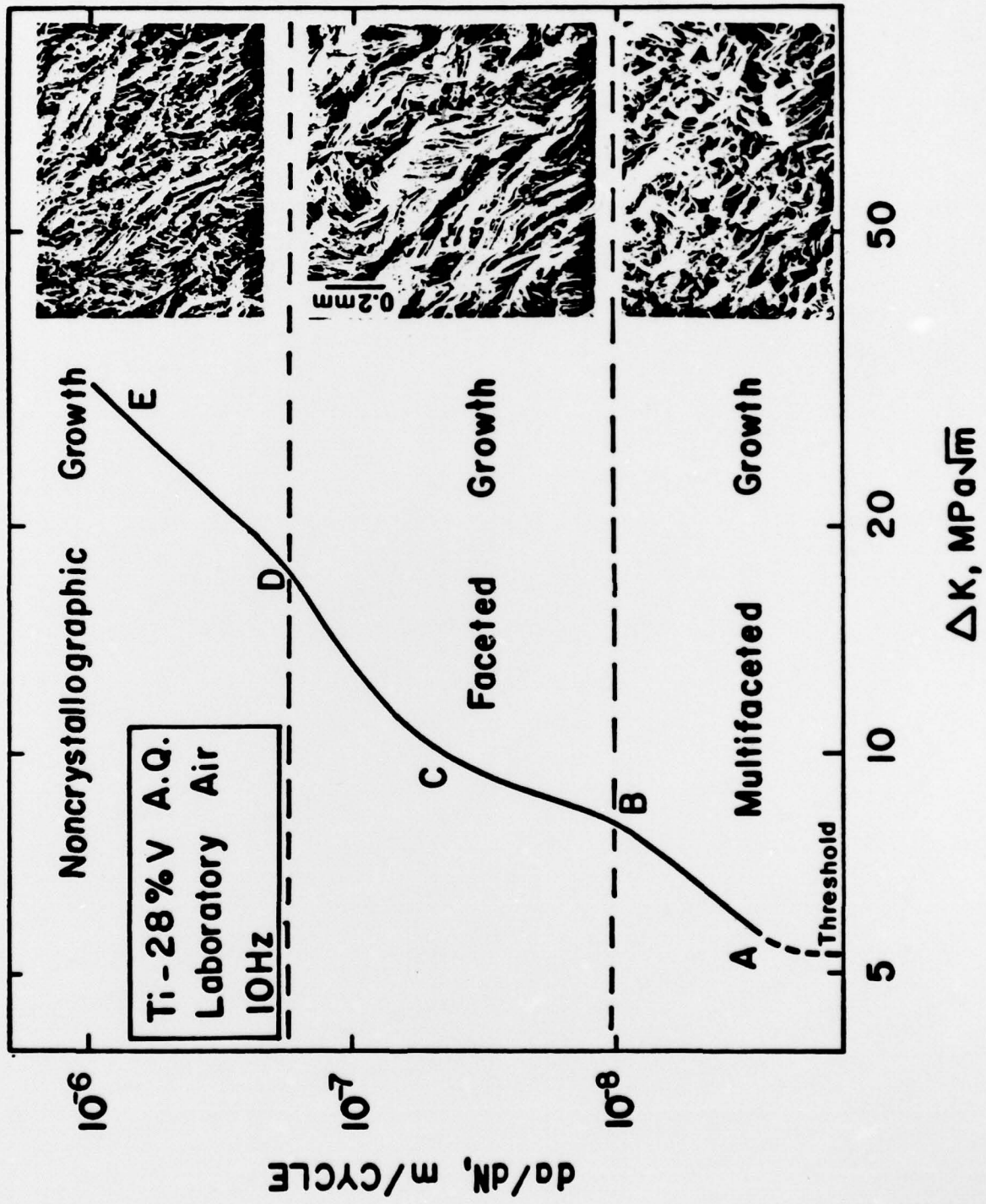
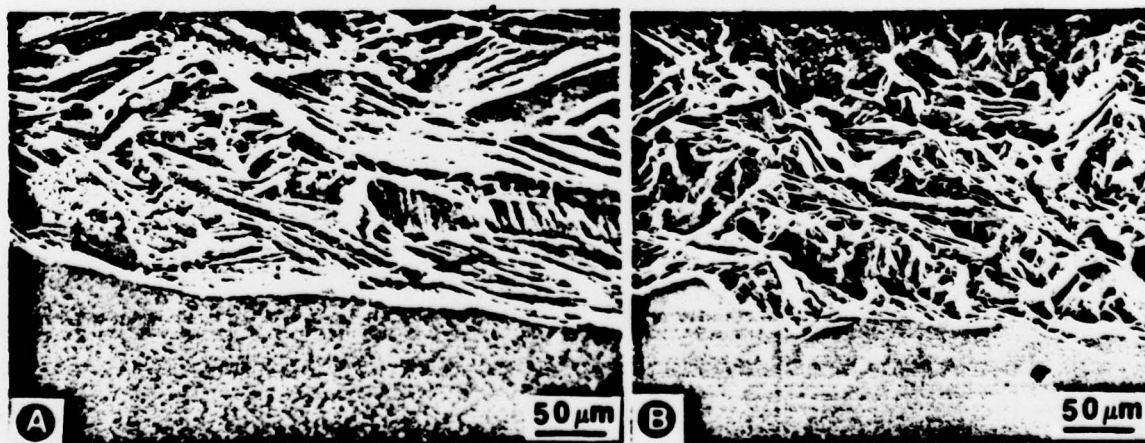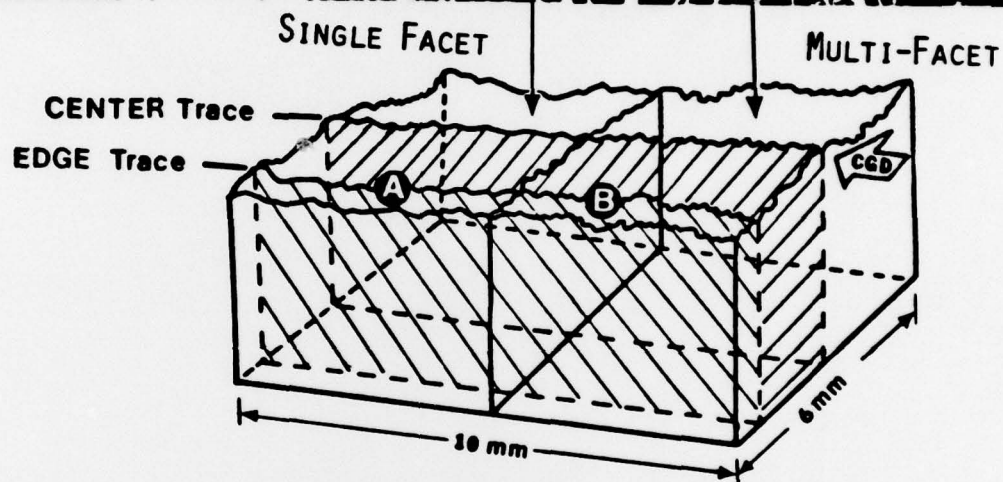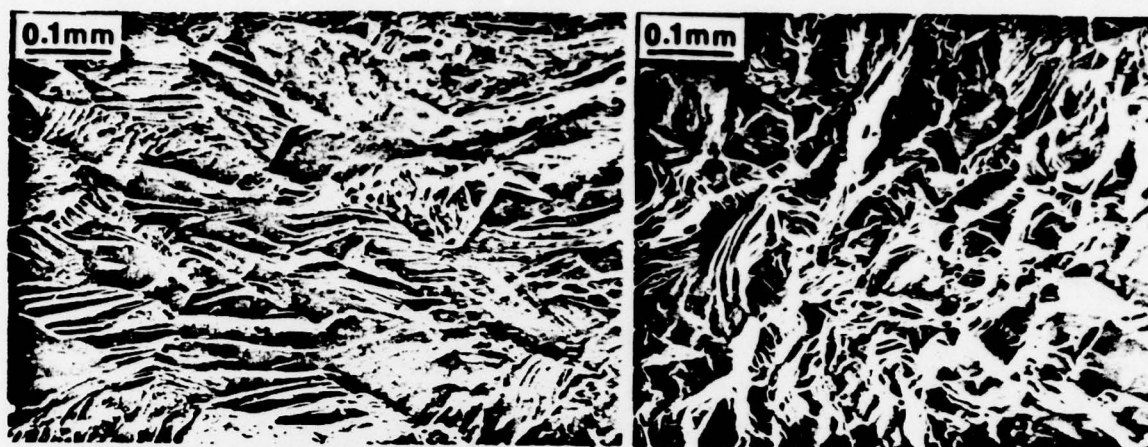## ACKNOWLEDGMENTS

REFERENCES

1. S. B. Chakrabortty, Fatigue of Engr. Mats. Structs., $\underline{2}$ (1979), to be published.

2. S. Majumdar and J. Morrow, ASTM STP No. 559 (1974) 159.

3. S. B. Chakrabortty and E. A. Starke, Jr., Met. Trans., $\underline{10A}$ (1979), to be published.

4. E. E. Underwood, Quantitative Stereology, Addison-Wesley (1970).

5. E. E. Underwood, Jnl. Micros., $\underline{95}$, Pt.1 (1972) 25.

6. Reference (4), Chapter 3, p. 48.

7. O. Johari, Res.-Dev., July (1971) 12.

8. J. E. Hilliard, Jnl. Micros., $\underline{95}$ Pt. 1 (1972) 45.

9. E. E. Underwood, The Microscope, 1st Q. (1974) 77.

10. R. C. Gifkins, Optical Microscopy of Metals, Pitman, London (1970).

11. B. K. P. Horn, Ph.D. Thesis, MIT (1970).

12. Reference (4), p. 189, p. 232.

13. V. A. Phillips, Modern Metallographic Techniques and Their Applications, Wiley-Interscience (1971).

14. Stereology, Proc. of Second Int. Congr. for Stereology, ed. by H. Elias, Springer-Verlag N.Y. (1967) see articles under "Reconstruction from Serial Sections" p. 293-324.

15. D. E. Passoja and D. C. Hill, ASTM STP No. 600 (1976).

16. R. H. Van Stone and T. B. Cox, ASTM STP No. 600 (1976) 5.

17. L. L.-J. Chin, Weld. Jnl., $\underline{48}$, Pt. 7 (1969) 290s.

18. J. R. Pickens and J. Gurland, Proc. Fourth Int. Congr. for Stereology, ed. by E. E. Underwood, R. deWit, and G. A. Moore, NBS Spec. Publ. 431 (1976) 269.

19. W. T. Shieh, Met. Trans. $\underline{5A}$, (1974) 1069.

20. D. Shechtman, Met. Trans., $\underline{7A}$, (1976) 151.

21. W. R. Kerr, D. Eylon and J. A. Hall, Met. Trans., $\underline{7A}$, (1976) 1477.

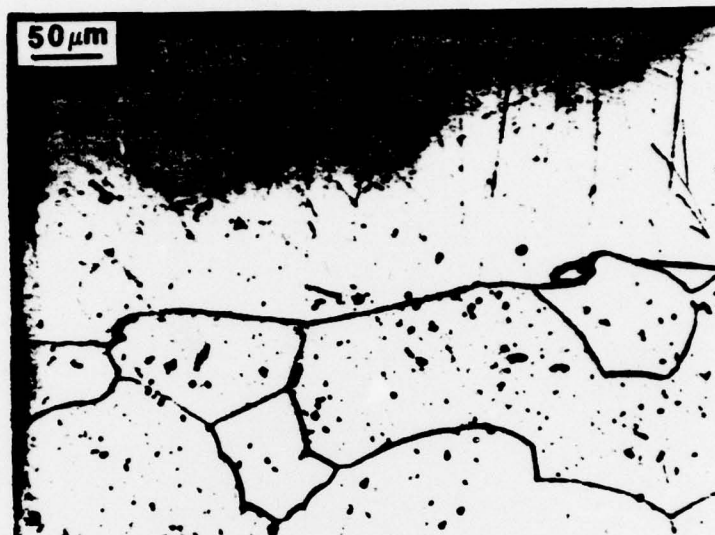22. E. A. Almond, J. T. King and J. D. Embury, Metallography, $\underline{3}$, (1970) 379.

23. J. C. Chesnutt and R. A. Spurling, Met. Trans., 8A, (1977) 216.

24. J.-L. Chermant and M. Coster, Jnl. Mats. Sci., 14, (1979) 509.

25. M. Coster and A. Deschanvers, Pract. Metallography, Spec. Vol. No. 8, ed. by J.-L Chermant, Dr. Riederer-Verlag, Stuttgart (1978) 61.

26. J.-L Chermant, M. Coster and A. Deschanvres, Metallography, 8, (1975) 271.

27. S. M. El-Soudani, Metallography, 7, (1974) 271.

28. S. M. El-Soudani, Metallography 11, (1978) 247.

29. E. E. Underwood and E. A. Starke, Jr., ASTM STP No. 675 (1979) 633.

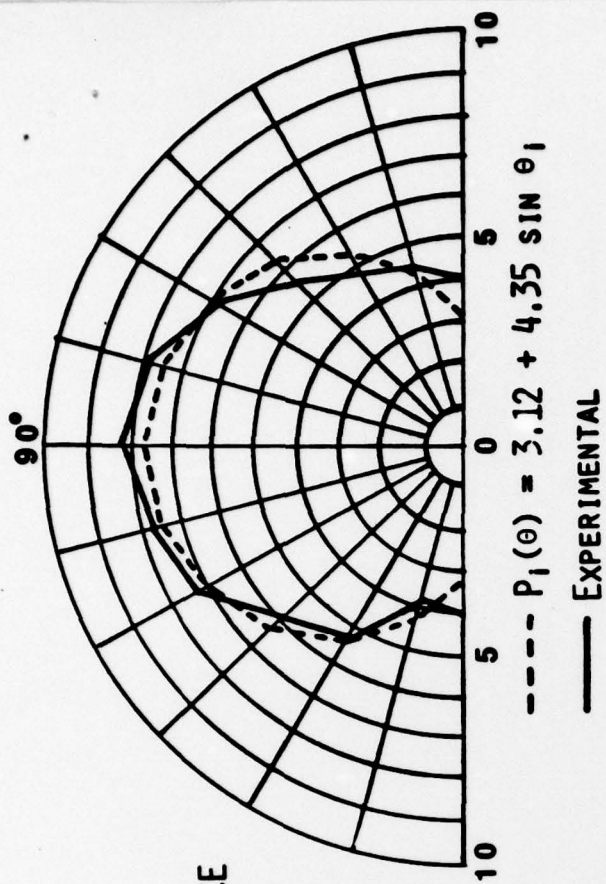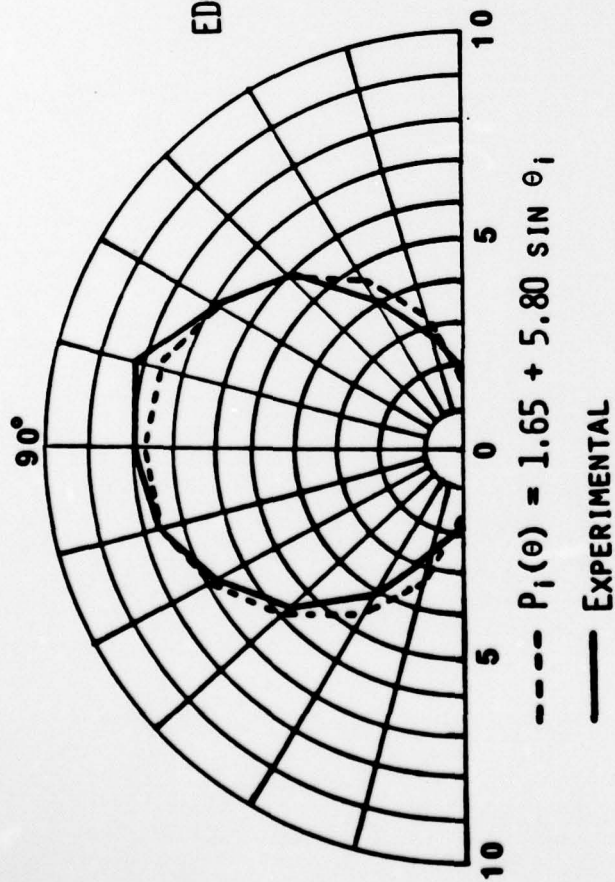30. H. Loeb, "The Role of Operator-Interactive Image Analysis Systems," Carl Zeiss, Inc., New York (1979).

FIGURE CAPTIONS

Figure 1. FCGR Curve for Ti-28 w/o V Alloy with SEM Pictures of Typical Fracture Appearance in Three Crack Growth Regions.

Figure 2. Over-view of Specimen Geometry Showing Fracture Surface, Edge and Center Traces, and Single-Facet and Multi-Facet Regions, Including Typical Views of Fracture Surfaces and Edge Trace by Oblique SEM.

Figure 3. Examples of Fracture Profile from Edge Vertical Section. (a) Single-Facet Region, (b) Multi-Facet Region. Note Copper Coating Above Fracture Traces, and Sub-Surface Cracks in (b).

Figure 4. Experimental and Least-Squares Polar Plots of the Rose, $P_i(\theta)$, for Edge and Center Traces.

Figure 5. Lineal Roughness Parameter, R_L, for Fracture Surface Traces Along Edge and Center Sections.

Figure 6. Upper and Lower Bounds of Fracture Roughness Parameter S_A in Single- and Multi-Facet Regions. Best Values for S_A, 1.32 in Single-Facet Region and 1.45 in Multi-Facet Region, Indicated by Arrows.

Figure 7. Variation of True Mean Facet Areas, $\bar{A}_{facets}$, in Single- and Multi-Facet Regions.

Figure 8. Lineal Crack Roughness Parameter, $(R_L)_{cracks}$, for Sub-Surface Crack Traces Along Edge and Center Sections.
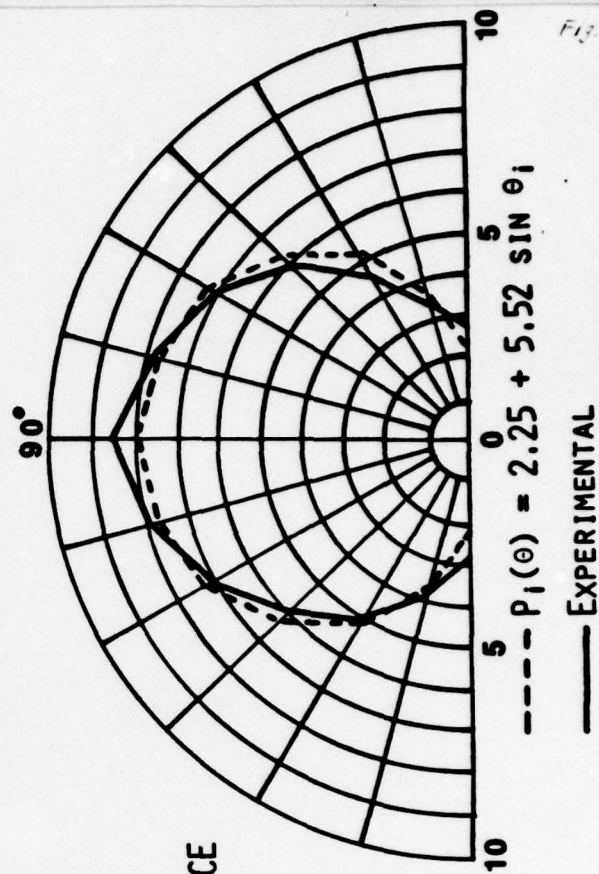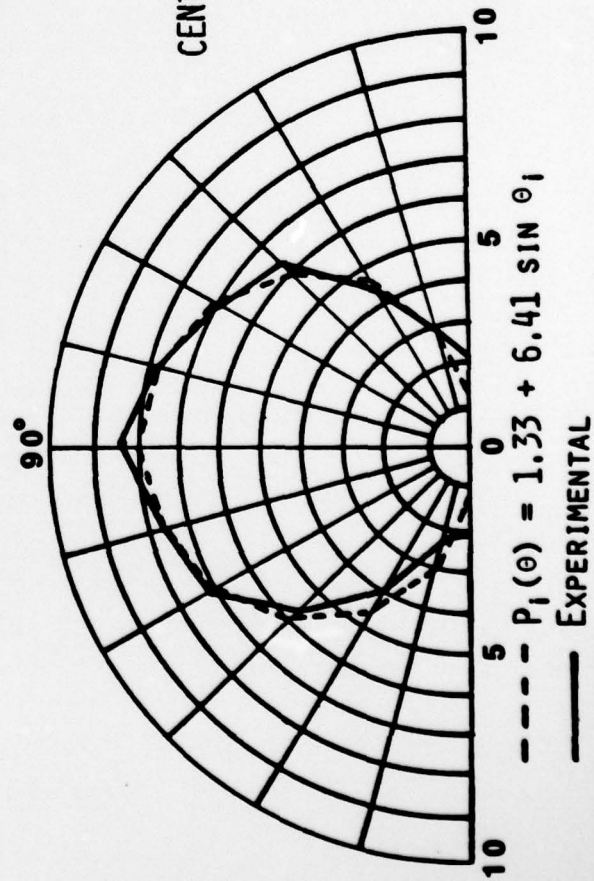
Fig. 1

SINGLE FACET   MULTI-FACET

CENTER Trace
EDGE Trace

Fig. 3

50 μm

50 μm

EDGE TRACE

$P_i(\Theta) = 3.12 + 4.35 \sin \Theta_i$
EXPERIMENTAL

MULTI-FACETS

CENTER TRACE

$P_i(\Theta) = 2.25 + 5.52 \sin \Theta_i$
EXPERIMENTAL

$P_i(\Theta) = 1.65 + 5.80 \sin \Theta_i$
EXPERIMENTAL

SINGLE FACETS

$P_i(\Theta) = 1.33 + 6.41 \sin \Theta_i$
EXPERIMENTAL

Fig 5

Fig 6

TOTAL CRACK LENGTH, mm

Fig. 7

Fig 8